The Astronomical Journal, 166:27 (11pp), 2023 July https://doi.org/10.3847/1538-3881/acd93a

The 14 Her Planetary System: Companion Masses and Architecture from Radial Velocities and Astrometry

G. F. Benedict[1], B. E. McArthur[1], E. P. Nelan[2], and J. L. Bean[3]
[1] McDonald Observatory, University of Texas, Austin, TX 78712, USA
[2] Space Telescope Science Institute, Baltimore, MD 21218, USA
[3] Department of Astronomy & Astrophysics,University of Chicago, Chicago, IL 60637, USA
Received 2023 April 8; revised 2023 May 13; accepted 2023 May 17; published 2023 June 26

Abstract

We combine Hubble Space Telescope (HST) Fine Guidance Sensor, Hipparcos, and Gaia DR3 astrometric observations of the K0 V star 14 Her with the results of an analysis of extensive ground-based radial velocity data to determine perturbation orbits and masses for two previously known companions, 14 Her b and c. Radial velocities obtained with the Hobby–Eberly Telescope and from the literature now span over 25 years. With these data we obtain improved radial velocity (RV) orbital elements for both the inner companion, 14 Her b and the long-period outer companion, 14 Her c. We also find evidence of an additional RV signal with $P \sim 3789^{\rm d}$. We then model astrometry from Hipparcos, HST, and Gaia with RV results to obtain system parallax and proper motion, perturbation periods, inclinations, and sizes due to 14 Her b and c. We find $P_{\rm b} = 1767.6 \pm 0.2$ days, perturbation semimajor axis $\alpha_{\rm b} = 1.3 \pm 0.1$ mas, and inclination $i_{\rm b} = 36° \pm 3°$, $P_{\rm c} = 52160 \pm 1028$ days, perturbation semimajor axis $\alpha_{\rm c} = 10.3 \pm 0.7$ mas, and inclination $i_{\rm c} = 82° \pm 14°$. In agreement with a past investigation, the 14 Her b, c orbits exhibit significant mutual inclination. Assuming a primary mass $M_* = 0.98 \pm 0.04 M_\odot$, we obtain companion masses $\mathcal{M}_{\rm b} = 8.5^{+1.0}_{-0.8}\ \mathcal{M}_{\rm Jup}$ and $\mathcal{M}_{\rm c} = 7.1^{+1.0}_{-0.6}\ \mathcal{M}_{\rm Jup}$.

Unified Astronomy Thesaurus concepts: Exoplanets (498)

Supporting material: machine-readable tables

1. Introduction

Exoplanetary systems provide an opportunity to probe the dynamical origins of planets (e.g., Ford 2006) and system evolution (Wright et al. 2009). They provide laboratories within which to tease out the essential processes and end states from the accidental. The nearby, metal-rich KO V star, 14 Her (HD 145675), has long been known to host a companion (Butler et al. 2003), and likely hosts a second (Goździewski et al. 2006; Wittenmyer et al. 2007; Wright et al. 2007; Hirsch et al. 2021; Rosenthal et al. 2021). Recent astrometric and radial velocity (RV) explorations of the 14 Her multiplanet system include Bardalez Gagliuffi et al. (2021) and Feng et al. (2022).

Before it was included in lists of multiplanet systems, we included 14 Her in a Hubble Space Telescope (HST) proposal (Benedict 2005) to carry out astrometry using the Fine Guidance Sensors (FGS). Those observations supported attempts to establish true component mass of several promising candidate systems, all relatively nearby, and with companion $\mathcal{M} \sin i$ values and periods suggesting measurable astrometric amplitudes. See Benedict et al. (2017), Section 4.6, for a review. As discussed below, these 14 Her FGS data were problematical, and until now, not fully analyzable.

We now return to these older FGS data, motivated by newer predictive resources. These include the Gaia DR3 Renormalized Unit Weight Error (RUWE) parameter, which predicts unmodeled photocenter motion (Stassun & Torres 2021) and the Brandt (2021) χ^2 value. The latter parameter measures an amount of measured acceleration obtained by comparing an earlier epoch proper motion from Hipparcos with a DR3 proper motion. A larger χ^2 value indicates more significant change (acceleration) in proper motion, thus a higher probability of a perturbing companion. For 14 Her $\chi^2 = 1009$ and RUWE = 1.819, both indicating significant difference from straight line motion.

14 Her is a system for which accurate component masses would prove useful. For 14 Her we use models previously employed for the exoplanet candidate systems ϵ Eri (Benedict et al. 2006), HD 33636 (Bean et al. 2007), υ And (McArthur et al. 2010), HD 136118 (Martioli et al. 2010), HD 38529 (Benedict et al. 2010), HD 128311 (McArthur et al. 2014), HD 202206 (Benedict & Harrison 2017), and μ Ara (Benedict et al. 2022b). A mass for 14 Her b was our original goal. Returning to this target, now with a suspected second companion, raises the possibility of establishing two companion masses and system architecture.

Section 2 identifies the sources of RV data and our RV modeling results for components 14 Her b and c. Section 3 describes the astrometric data and modeling techniques used in this study, now enabled by reference star astrometry from the Gaia DR3 catalog, and ICRS positions for 14 Her from Hipparcos, Gaia DR1, and DR3. Including orbits for 14 Her b and c, informed by orbital priors from the RV analysis, yields orbital elements and masses (Section 4). We compare our results with previous investigations, and place them in the context of past FGS astrometric results (Section 5). Lastly, in Section 6 we summarize our findings.

For this investigation we adopt the 14 Her stellar properties presented in Table 1 of Bardalez Gagliuffi et al. (2021), most critically the host star mass, $\mathcal{M}_\star = 0.98 \pm 0.04\ \mathcal{M}_\odot$. For our assessment of the reality of candidate companion 14 Her d, we

Table 1
The RV Data Sets

Data Set	Coverage	Nobs	Rms (m s^{-1})	RV ZP (m s^{-1})[a]
ESO	1995.09–2003.59	117	9.9	72.3 ± 1.2
Keck	2004.64–2020.15	231	3.3	0
HET	2006.04–2008.31	77	4.9	5.4 ± 0.6
APF	2014.01–2019.28	208	3.8	-18.4 ± 0.2
	total	684		

Note.
[a] RV zero-point adjustment values relative to Keck.

also adopt from their Table 1 an activity parameter, $\log R'_{\rm HK} = -4.94 \pm 0.04$, a rotation period, $P_{\rm rot} = 29\overset{\rm d}{.}5$, and an age estimate of $4.6^{+3.8}_{-1.3}$ Gyr.

We abbreviate millisecond of arc as mas throughout and state times as mJD = JD–2400000.5.

2. Radial Velocities

Sources (Table 1) of RV data include previously published ELODIE (Naef et al. 2004), the Automated Planet Finder (APF) at Lick Observatory (Vogt et al. 2014), and Keck HIRES (Butler et al. 2003; Wittenmyer et al. 2007; Hirsch et al. 2021; Rosenthal et al. 2021). The Hobby–Eberly Telescope High Resolution Spectrograph (Tull 1998) provided previously unpublished measurements, produced using the pipeline described in Bean et al. (2007).

All four sources of relative RV have differing zero-points. Our modeling includes zero-point offsets as solved-for parameters, listed in Table 1, where we have arbitrarily assumed a 0.0 zero-point for the Keck data. Because our GaussFit (Jefferys et al. 1988) modeling results critically depend on the input data errors, we first modeled the RV to assess the validity of the original input RV errors. In order to achieve a χ^2/DOF of unity for our solution required increasing the original errors on the RV by a factor of 2.9 for all sources. This suggests that either the errors were underestimated, or that that the fit is not as good as it could be (i.e., evidence that there may be more to learn about the system), or a level of stellar-induced RV noise.

Figure 1 presents RV plotted as a function of time and the final combined orbital solution. Table 2 lists the final zero-point corrected RV, along with our scaled errors. Table 1 also includes the rms residual for each source. Table 3 contains orbital elements and 1σ errors for 14 Her b,c.

We remove the 14 Her c RV orbit from the combined fit and phase the resulting RV (Figure 2, top) to the 14 Her b orbital period. The bottom panel presents RV with component b subtracted, phased to the Table 3 14 Her c period. The red boxes in each panel indicate phases at which FGS astrometry took place, and for the Hipparcos, Gaia DR1, and Gaia DR3 observations.

The residuals in Figure 1 suggests a periodic pattern. A Lomb–Scargle periodogram of these residuals, after removing the RV contributions from 14 Her b, and c, displays a very strong peak at $P \sim 3790^{\rm d}$. We were able to determine the orbit-like parameters listed in Table 4 from these very noisy $\rm RV_d = RV_{all} - RV_b - RV_c$. We also list parameters for a simple sine wave fit

$$\rm RV = K * \sin(((2\pi/P) * mJD) + \phi)) \quad (1)$$

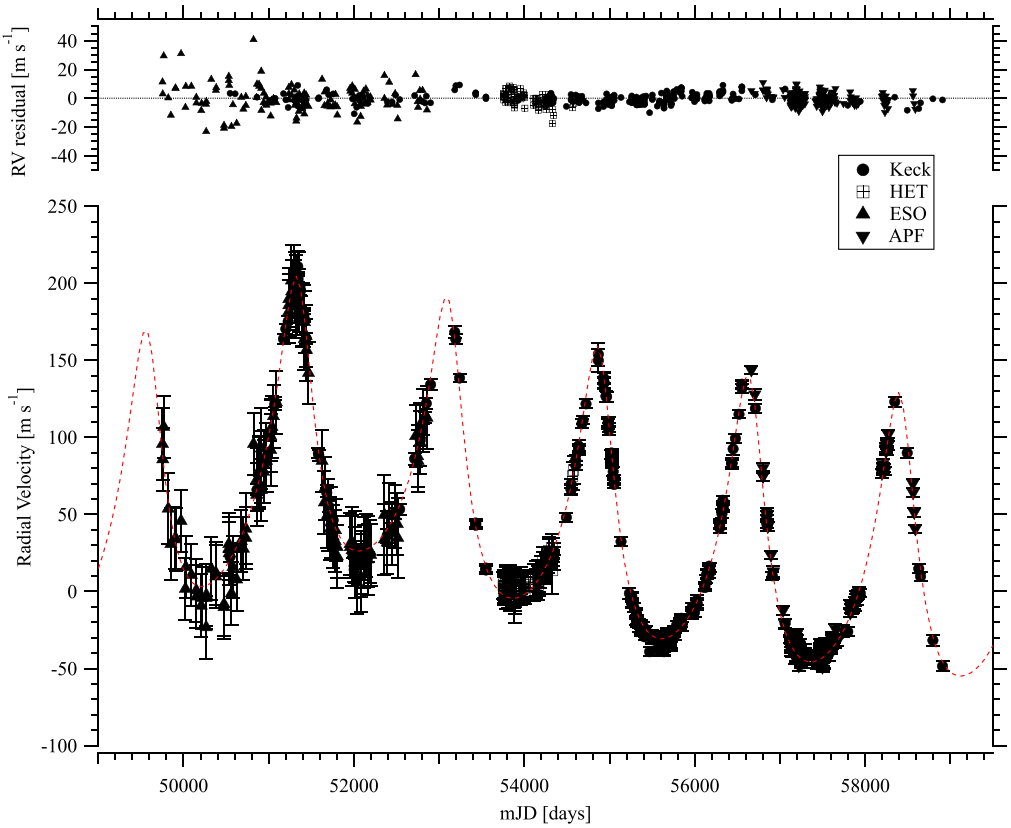

Figure 1. RV values and 1σ errors from the sources listed in Table 1 plotted on the final RV two component orbit (Table 3). All RV input errors have been increased by a factor of 2.9 to achieve a near unity χ^2/DOF. Residuals are plotted in the top panel. We note the rms RV residual values for each source in Table 1.

Table 2
RV Data[a]

mJD	RV (m s^{-1})	±error[b]	Source[c]
53752.5331	3.9	8.9	HET
53753.5069	3.2	9.0	HET
53754.4962	4.8	9.2	HET
53755.5097	1.9	9.0	HET
53756.5094	0.1	9.0	HET
53764.4816	2.3	8.9	HET
53766.4967	1.8	8.9	HET
53768.4681	3.5	8.8	HET
53778.4754	7.3	8.8	HET
53780.4533	−2.3	8.8	HET
53787.4326	7.1	10.1	HET
53794.4119	0.1	8.9	HET
53800.3741	−2.2	8.8	HET
53808.3481	2.4	9.3	HET

Notes.
[a] Full table available online.
[b] Errors adjusted to achieve χ^2/DOF near unity.
[c] HET = Hobby–Eberly Telescope, ESO = ELODIE, Keck = HIRES, APF = Automatic Planet Finder.
(This table is available in its entirety in machine-readable form.)

Table 3
14 Her b,c Orbital Parameters from RV

Parameter	b	c
P [days]	1767.8 ± 0.6	52172 ± 2326
P [yr]	4.840 ± 0.002	143 ± 6
T[a] [days]	51368 ± 2	51781 ± 73
e	0.372 ± 0.003	0.63 ± 0.01
ω (°)	22.3 ± 0.4	−2 ± 2
K (m s^{-1})	90.3 ± 0.4	51 ± 1

Note.
[a] $T = T$–2400000.5.

to these same data. The two fits have similar χ^2 values. Figure 3 contains system RV with 14 Her b,c orbits subtracted, phased to $P = 3765$, fit to the Table 4 sine wave. Hirsch et al. (2021) identify a periodic signal at 3440^d that they interpret as a stellar activity cycle. To interpret the $P \sim 3790^d$ signal as planetary in origin is premature. See Benedict et al. (2010) and Henry et al. (2013) to appreciate the value of continued RV monitoring in regards to the interpretation of low-amplitude signals, and witness the demise of HD 38529d.

3. Astrometry

3.1. Astrometric Data

For this study astrometric measurements came from Fine Guidance Sensor 1r (FGS 1r), an upgraded FGS installed in 1997 during the second HST servicing mission, from Gaia DR1 (Lindegren et al. 2016), DR3 (Gaia Collaboration et al. 2022), and from Hipparcos (van Leeuwen 2007).

3.1.1. FGS Data

We utilized the fringe tracking mode (POS mode; see Benedict et al. 2017 for a review of this technique) in this investigation. POS-mode observations of a star have a typical

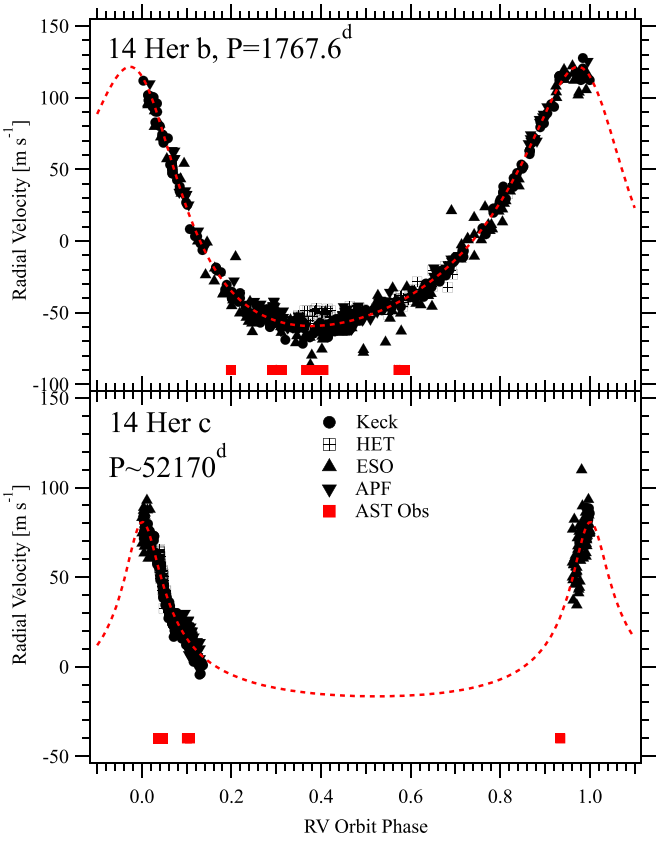

Figure 2. RV measurements of 14 Her from sources as indicated in the legend (and identified in Table 1) phased to the orbital periods determined from RV (Section 2). The dashed line is the RV predicted from the orbital parameters (Table 3). The red boxes denote corresponding phases of Hipparcos, FGS, DR1, and DR3 astrometry.

Table 4
14 Her d Orbital and Sin Wave Parameters from RV

Parameter	Orbit	Sin Wave
P [days]	3765 ± 77	3789 ± 71
T [days]	56425 ± 183	⋯
e	0.17 ± 0.06	⋯
ω[a] (°)	−47 ± 18	52 ± 2
K (m s^{-1})	3.8 ± 0.2	3.5 ± 0.2

Note.
[a] ϕ in Equation (1).

duration of 60 s, during which over two thousand individual position measurements are collected. We estimate the astrometric centroid by choosing the median measure, after filtering large outliers (caused by cosmic ray hits and particles trapped by the Earth's magnetic field). The standard deviation of the measures provides a measurement error. We refer to the aggregate of astrometric centroids of each star secured during one visibility period (typically on order 40 minutes) as a "set." We identify the astrometric reference stars and science target in Figure 4.

Table 5 lists mJD for all astrometry used in this investigation. These FGS data suffer from several deficiencies, which up until Gaia, have rendered them unable to produce the proposed (Benedict 2005) result; that of a mass estimate for 14 Her b. First, these data, collected from 2005.84 to 2007.19, are significantly bunched, and provide for a companion period,

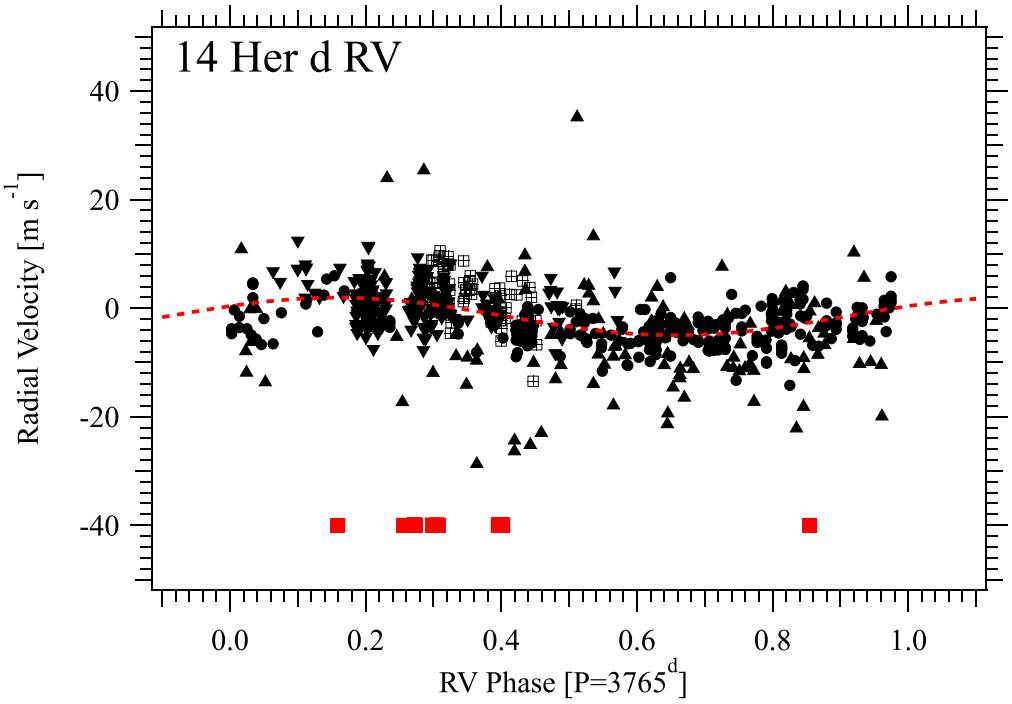

Figure 3. Candidate component d RV orbit (Table 4) obtained from the $RV_d = RV_{all} - RV_b - RV_c$, phased to the Table 4 orbit period. A sine wave fit is plotted. RV source symbols from Figure 2. The red boxes denote corresponding phases of Hipparcos, FGS, DR1, and DR3 astrometry.

$P > 4.5$ yr, effectively only three observational epochs: sets 1–6, sets 7–9, and sets 10–17. Second, HST gyro problems (see Benedict et al. 2010, Section 3, for details) required that we switch astrometric reference frames during our sequence of scheduled observations. Sets 1–6 included 14 Her and reference stars 30–35. Sets 7–17 included 14 Her, reference star 34, and reference stars 61–65.

3.1.2. Gaia DR3

To address both these problems, we incorporate three epochs of 14 Her astrometry from Hipparcos, Gaia DR1, and DR3, and all reference star positions from Gaia DR3. To use them with the FGS data we derive standard coordinates, ξ, η, for reference stars and 14 Her ICRS 2016.0 positions provided by DR3. Table 6 contains those epoch 2016.0 positions. We also list the RUWE for each reference star. Stassun & Torres (2021) find that the Gaia RUWE robustly predicts unmodeled photocenter motion, even in the nominal "good" range of 1.0–1.4. Following van de Kamp (1967),

$$\xi = \frac{\cos\delta \sin\Delta\alpha}{(\sin\delta \sin\delta_0 + \cos\delta \cos\delta_0 \cos\Delta\alpha)} \quad (2)$$

$$\eta = \frac{\sin\delta \cos\delta_0 - \cos\delta \sin\delta_0 \cos\Delta\alpha}{\sin\delta \sin\delta_0 + \cos\delta \cos\delta_0 \cos\Delta\alpha} \quad (3)$$

where α, δ are R.A., decl., α_0, δ_0 are the position of the tangent point of the field (taken to be the average R.A. and decl. of the target and reference stars in Table 6), and $\Delta\alpha$ the R.A. distance from the tangent point for each star. The FGS astrometry pipeline produces standard coordinates in arc seconds. Hence, the DR3 ξ, η in radians are transformed to arc seconds. We derive the 14 Her Hipparcos and DR1 epoch by producing a difference (in arc seconds) between the DR3 ICRS position and the Hipparcos and DR1 ICRS positions.

The Gaia DR3 standard coordinates now constitute our master constraint plate. For past investigations we chose one of the FGS data sets as a master constraint plate. This did not work for our aggregate 14 Her field data, given that the only stars in common to all FGS sets were 14 Her and reference star 34. The Gaia DR3 field contains all stars. We present DR3 reference star standard coordinates and a complete ensemble of FGS time-tagged 14 Her and reference star astrometric measurements, OFAD[4]- and intra-orbit drift-corrected, in Table 7, along with calculated parallax factors in R.A. and decl. The Hipparcos and DR1 14 Her positions, and the DR3 14 Her and reference star positions are ICRS barycentric, hence, require no parallax factors.

3.1.3. Gaia DR1 and Hipparcos

For 14 Her only we include ICRS positions from Gaia DR1 (Lindegren et al. 2016) and Hipparcos (van Leeuwen 2007). The latter extends the span of astrometry to 24.75 yr. These measurements enter Table 7 as offsets from the DR3 ICRS position.

3.2. Astrometry Modeling Priors

As in all of our previous FGS astrometry projects, e.g., Benedict et al. (2001, 2007, 2011, 2016, 2022a, 2022b), Bean et al. (2007), Martioli et al. (2010), McArthur et al. (2010, 2014), and Benedict & Harrison (2017), we include as much prior information as possible in our modeling.

We employ the following priors:

1. *Parallax:* this investigation adopts DR3 values (Gaia Collaboration et al. 2022). As in past investigations, we do not treat those values as being hardwired or absolute.

[4] The Optical Field Angle Distortion (OFAD) calibration (McArthur et al. 2006).

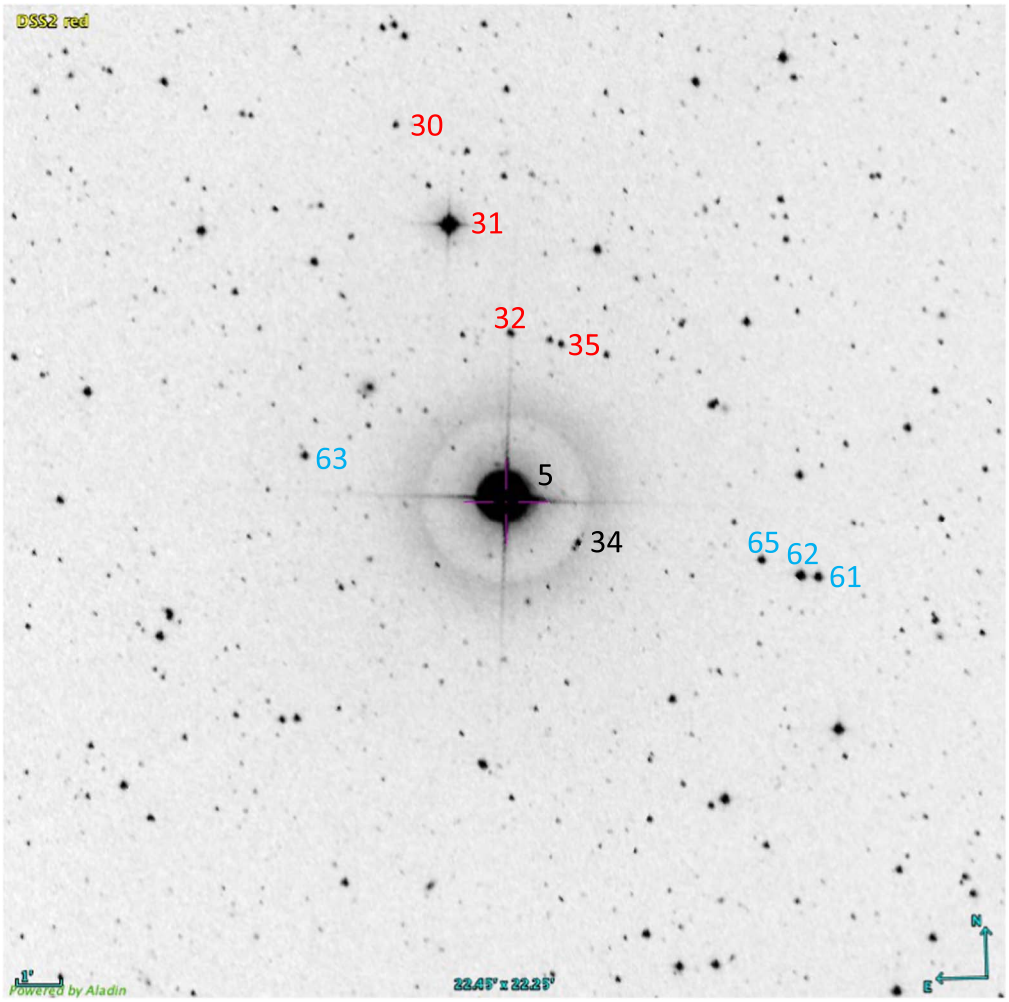

Figure 4. Positions of 14 Her (5) and astrometric reference stars. The FGS observed stars with red ID numbers in sets 1–6, and stars with blue IDs in sets 7–17. Due to HST gyro issues, 14 Her and ref-34 were the only two stars observed in each set. The Gaia DR3 set 18 includes 14 Her and all reference stars.

Instead, we consider them to be quantities (Table 8) introduced as observations with error. The average DR3 parallax error is 0.02 mas. Note that we utilize no parallax prior for 14 Her, an independent parallax having some value.

2. *Proper Motions:* for the reference stars we use the Table 8 proper motion priors from DR3 with median errors $\sigma_\mu \simeq 0.014$ mas. Simply relying on the DR3 values for 14 Her might introduce a bias, given the limited DR3 time span and the potentially complicated perturbations from the known components. We utilize no proper motion priors for 14 Her.
3. *Lateral Color Corrections:* these corrections, entered into the model as data with errors, are identical to those used in Benedict & Harrison (2017). The $B-V$ values (Table 6) come from measurements made with the New Mexico State University 1 m telescope (Holtzman et al. 2010).
4. *Cross Filter Corrections: FGS 1r* contains a neutral density filter, reducing the brightness of 14 Her by five magnitudes (from $V = 6.6$ to $V = 11.6$), permitting simultaneous modeling of 14 Her with far fainter reference stars with $\langle V \rangle = 12.8$. These corrections, entered into the model as data with errors, are identical to those used in Benedict & Harrison (2017).

3.3. Modeling the 14 Her Astrometric Reference Frame

The astrometric reference frame for 14 Her consists of nine stars (Table 6). The 14 Her field (Figure 4) exhibits the distribution of astrometric reference stars (ref-30 through ref-65) used in this study. Due to HST gyro difficulties, (see Benedict et al. 2010, Section 3, for details), the 14 Her field was observed at a very limited range of spacecraft roll values (Table 7). At each epoch we measured each available reference star 1–4 times, and 14 Her 3–5 times. Given the distribution of reference stars, FGS 1r could observe only ref-34 and the science target, 14 Her, at each epoch. The inclusion of a constraint plate derived from the Gaia DR3 catalog permits the following astrometric analysis.

Our choice of model (Equations (5)–(6)) was driven entirely by the goodness of fit for the reference stars. We used no 14 Her observations to determine the reference frame mapping coefficients, $A-F$. We solve for roll, offsets, and independent scales along each axis.

3.4. The Model

From positional measurements we determine the scale, rotation, and offset "plate constants" relative to our adopted constraint epoch (Gaia DR3 ICRS 2016.0) for each observation set. We employ GaussFit (Jefferys et al. 1988) to minimize χ^2.

Table 5
Log of 14 Her Astrometry Observations

Set	mJD
1	53681.092
2	53682.954
3	53683.886
4	53684.885
5	53685.883
6	53686.881
7	53786.216
8	53804.872
9	53813.938
10	54150.063
11	54150.992
12	54152.060
13	54157.718
14	54163.045
15	54168.705
16	54171.102
17	54172.633
18[i]	48347.313
18[ii]	57023.000
18[iii]	57388.000

Notes.
[i] ICRS epoch 1991.25 from Hipparcos.
[ii] ICRS epoch 2015.0 from Gaia DR1.
[iii] ICRS epoch 2016.0 from Gaia DR3.

The solved equations of condition for the 14 Her field are:

$$x' = x + lc_x(B - V) - \Delta XF_x \quad (4)$$

$$y' = y + lc_y(B - V) - \Delta XF_y \quad (5)$$

$$\xi = Ax' + By' + C - \mu_\alpha \Delta t - P_\alpha \varpi - \sum_{n=1}^{2} O_{n,x} \quad (6)$$

$$\eta = Dx' + Ey' + F - \mu_\delta \Delta t - P_\delta \varpi - \sum_{n=1}^{2} O_{n,y}. \quad (7)$$

Identifying terms, x and y are the measured coordinates from HST; $(B - V)$ is the Johnson $(B - V)$ color of each star; lc_x and lc_y are the lateral color corrections; and ΔXF_x and ΔXF_y are cross filter corrections applied only to 14 Her. A, B, D, E, are scale and rotation plate constants; C and F are offsets; μ_α and μ_δ are proper motions; Δt is the time difference from the constraint plate epoch; P_α and P_δ are parallax factors from a JPL Earth orbit predictor (Standish 1990), version DE405; and ϖ is the parallax. O_x and O_y, shown here for a two component planetary system, are functions of the classic orbit parameters: α, the perturbation semimajor axis; i, inclination; ϵ, eccentricity; ω, argument of periastron; Ω, longitude of ascending node; P, orbital period; and T, time of periastron passage for each included component (Heintz 1978). ξ and η are relative positions in R.A. and decl. that (once scale, rotation, parallax, the proper motions, and the O are determined) should not change with time.

At this stage we model *only* astrometry and *only* the reference stars. From histograms of the reference frame model astrometric residuals (Figure 5) we conclude that we have a well-behaved reference frame solution exhibiting residuals with Gaussian distributions with dispersions $\sigma_{(x,y)}$=0.9, 0.6 mas. A reference frame "catalog" from FGS 1r and DR3 in ξ and η standard coordinates was determined with average uncertainties, $\langle\sigma_\xi\rangle = 0.07$ and $\langle\sigma_\eta\rangle = 0.07$ mas. Because our constraint plate consists of Gaia DR3 R.A., decl., ξ and η are R.A. and decl. Note that we removed ref-61 from the DR3 constraint plate due to its very high RUWE value (Table 6). The behavior of the ref-61 FGS 1r residuals indicate nothing systematic, other than having the largest final positional uncertainties, $\sigma_\xi = 0.57$ and $\sigma_\eta = 0.53$ mas. Lastly, we obtained a final reference frame mapping by removing ref-30. This resulted in a 55% reduction in χ^2, compared to including that reference star.

At this step in the analysis the astrometry knows nothing of the RV detections (Table 3). With our derived A, B, D, E, C, and F we transform the 14 Her astrometric measurements, applying A through F as constants, solving only for 14 Her proper motion and parallax, using no priors for 14 Her. Table 9 compares values for the parallax and proper motion of 14 Her from HST and Gaia (Gaia Collaboration et al. 2022). We note a significant disagreement in the proper motion vector ($\boldsymbol{\mu}$) absolute magnitude and the parallax values. This could be explained both by our nonglobal proper motion measured against a small sample of reference stars, and the limited

Table 6
Star Positions[i] from Gaia DR3

ID	R.A. (°)	R.A. err (mas)	Decl.(°)	Decl. err (mas)	G (mag)[ii]	RUWE[iii]	$B - V$[iv]
14 Her	242.6021268	0.02	43.8163208	0.03	6.40	1.819	0.87
30[v]	242.6577288	0.01	43.9581798	0.01	14.15	1.016	0.99
31	242.6305334	0.01	43.9208867	0.01	9.43	1.056	0.52
32	242.5982813	0.01	43.8801370	0.01	13.64	1.061	0.71
34	242.5643202	0.01	43.8021963	0.01	14.20	0.974	0.52
35	242.5725899	0.01	43.8758601	0.02	14.55	0.963	0.87
61[vi]	242.4391655	0.15	43.7893724	0.17	12.94	14.457	0.87
62	242.4481893	0.01	43.7898342	0.01	12.29	1.034	0.70
63	242.7050172	0.01	43.8342381	0.01	13.83	1.013	0.87
65	242.4685474	0.01	43.7949531	0.01	13.60	1.029	1.17

Notes.
[i] Epoch 2016.0 ICRS Positions from DR3.
[ii] G Magnitude from DR3; all errors 0.0028 mag.
[iii] Reduced Unit Weight Error.
[iv] All errors 0.03 mag.
[v] Not included in modeling due to high FGS residuals.
[vi] Not included in DR3 constraint plate due to high RUWE.

Table 7
14 Her Field Astrometry[a]

Set	Star	ID	Field Roll[b]	X	Y	σ_X	σ_Y	t_{obs}	P_α	P_δ
18	14 Her	DR3	0	86.96035	−107.53965	2.22E-05	2.68E-05	57388.0	0	0
18	14 Her	DR1	0	86.82854	−107.24292	2.12E-04	2.23E-04	57023.0	0	0
18	14 Her	HIPP	0	83.678864	−100.16482	2.7E-04	3.0E-04	48347.3	0	0
18	30	DR3	0	230.84356	403.26011	1.12E-05	1.18E-05	57388.0	0	0
18	31	DR3	0	160.46832	268.94001	1.02E-05	1.10E-05	57388.0	0	0
18	32	DR3	0	76.88882	122.19479	1.01E-05	1.11E-05	57388.0	0	0
18	34	DR3	0	−11.24992	−158.40539	1.22E-05	1.31E-05	57388.0	0	0
18	35	DR3	0	10.22438	106.78428	1.37E-05	1.52E-05	57388.0	0	0
18	62	DR3	0	−313.05087	−202.68143	9.10E-06	9.90E-06	57388.0	0	0
18	63	DR3	0	354.12504	−42.76332	1.04E-05	1.13E-05	57388.0	0	0
18	65	DR3	0	−260.12227	−184.32370	1.00E-05	1.13E-05	57388.0	0	0
1	5	F9D23701M[c]	159.836	−89.59243	−90.29798	2.22E-03	2.43E-03	53681.07782	−0.463950	−0.820011
1	5	F9D23707M	159.836	−89.59375	−90.29817	2.01E-03	2.32E-03	53681.0858	−0.463782	−0.820035
1	5	F9D2370DM	159.836	−89.59390	−90.29833	1.96E-03	2.25E-03	53681.0936	−0.463642	−0.820063
1	5	F9D2370HM	159.836	−89.59469	−90.29905	1.94E-03	2.41E-03	53681.09898	−0.463550	−0.820090
1	5	F9D2370LM	159.836	−89.59578	−90.29930	2.02E-03	2.35E-03	53681.10392	−0.463462	−0.820124
1	30	F9D23706M	159.836	437.31868	−52.27713	3.08E-03	2.53E-03	53681.08441	−0.466121	−0.820927
1	30	F9D2370CM	159.836	437.32002	−52.27917	2.96E-03	2.53E-03	53681.09221	−0.465977	−0.820953
1	30	F9D2370GM	159.836	437.31986	−52.27674	2.96E-03	2.57E-03	53681.09758	−0.465885	−0.820978
1	31	F9D23705M	159.836	286.70230	−32.58164	2.43E-03	2.04E-03	53681.0831	−0.465266	−0.820736
1	31	F9D2370BM	159.836	286.70385	−32.58115	2.46E-03	2.28E-03	53681.0909	−0.465119	−0.820761
...	...	...	...	...	...	...	...	...	...	...

Notes.
[a] Set (orbit) number, star number (#5 = 14 Her; reference star numbers same as Table 6), OFAD-corrected X and Y positions in arcsec, position measurement errors in arcsec, time of observation = JD–2400000.5, R.A. and decl. parallax factors. We provide a complete table in the electronic version of this paper. Set 18 from Hipparcos, Gaia DR1, and Gaia DR3; DR3 standard coordinates from Equations (1) and (2).
[b] DR3 assumed oriented to R.A., decl. HST orientation; spacecraft +V3 axis roll angle as defined in Chapter 2, FGS Instrument Handbook (Nelan 2015).
[c] HST orbit and target identifier.

(This table is available in its entirety in machine-readable form.)

Table 8
Reference Star Parallax and Proper Motion Priors from Gaia DR3

ID	ϖ (mas)	$\mu_{R.A.}$ (mas yr^{-1})	$\mu_{Decl.}$ (mas yr^{-1})
14 Her	55.87 ± 0.03	131.75 ± 0.03	−297.03 ± 0.04
30	0.22 0.01	−4.42 0.01	−10.37 0.02
31	7.63 0.01	−18.92 0.01	25.22 0.02
32	1.96 0.01	−0.26 0.01	−4.54 0.02
34	0.94 0.01	1.50 0.02	3.66 0.02
35	1.94 0.02	16.57 0.02	−26.78 0.02
61	2.82 0.18	0.58 0.19	0.72 0.21
62	3.07 0.01	−12.57 0.01	−0.92 0.01
63	0.67 0.01	−5.85 0.01	−2.03 0.02
65	6.21 0.01	−8.32 0.01	−29.79 0.01

duration of both astrometric studies, possibly affected by the companion perturbations. Alternatively, the mismatch between our proper motion, established through measurements taken from 1991.25 (Hipparcos), 2005.84 to 2007.19 (FGS), and the Gaia DR1 and DR3 values, a result of a campaign spanning 2014.6–2017.4, could indicate acceleration due to the companions, as might the RUWE = 1.82. Furthermore, Brandt (2021) finds a very high $\chi^2 > 1000$ when solving a model assuming no proper motion change, comparing Hipparcos with Gaia, indicating significant 14 Her acceleration over a roughly 25 yr time span.

4. Perturbation Orbits and Mass Estimates

4.1. 14 Her b,c

We next employ Equations (7)–(8), looking for astrometric evidence of 14 Her b and c. With our derived A, B, D, E, C, and F we transform the 14 Her astrometric measurements, applying A through F as constants, now solving for 14 Her proper motion, parallax, and b, c orbits, again, using no parallax and proper motion priors for 14 Her. We force astrometry and RV to describe the same perturbation through a constraint (e.g., Pourbaix & Jorissen 2000) for a perturbing companion

$$\frac{\alpha_b \sin i_b}{\varpi_{abs}} = \frac{P_b K_b (1 - e_b^2)^{1/2}}{2\pi \times 4.7405}. \quad (8)$$

Using 14 Her b as an example, Equation (8) contains quantities derived from astrometry (parallax, ϖ_{abs}, host star perturbation orbit size, α, and inclination, i) on the left-hand side, and quantities derivable from both (the period, P, and eccentricity, ϵ), or only radial velocities (the RV amplitude of the primary, K, induced by a companion), on the right-hand side.

The RV provide far higher cadence coverage of the 14 Her b and c perturbations than do the far sparser astrometric measurements, providing essential support for determining P, ϵ, K, ω, and T. For these orbit determinations, we introduce the Table 3 RV-provided values as observations with error. We use the Equation (8) relationship between the astrometry and the RV, but hold no orbital or astrometric parameters as constants. Our solutions do not converge unless there is a measurable signal. Table 10 contains the resulting orbits. For 14 Her b the

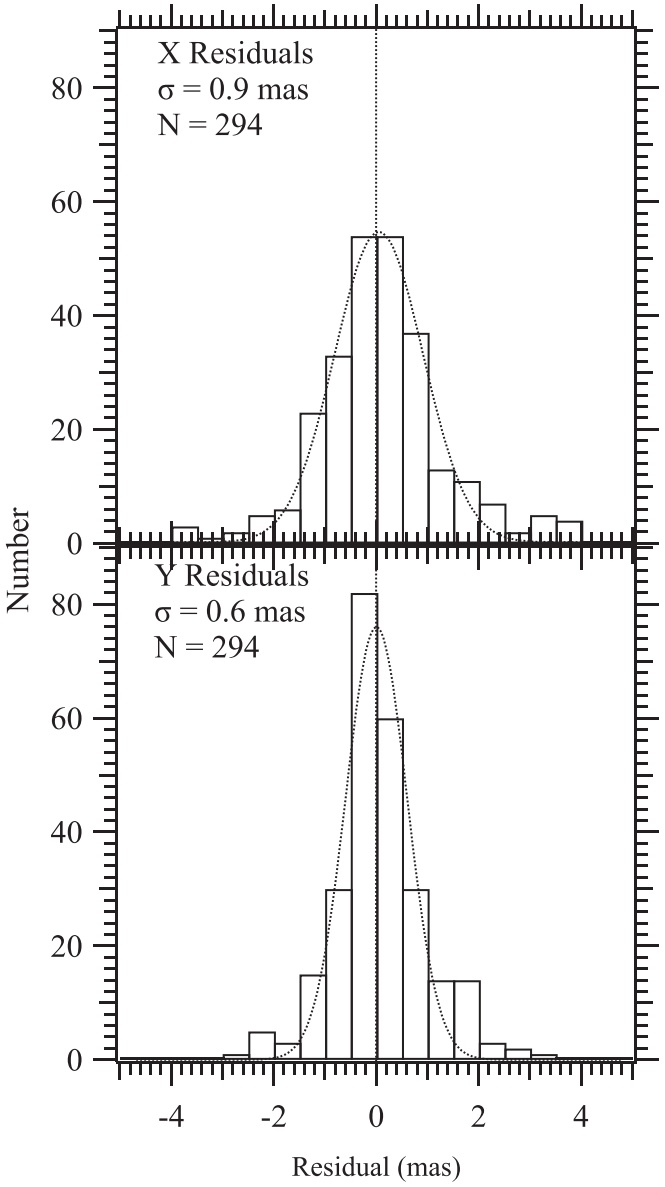

Figure 5. Histograms of x and y residuals obtained by deriving the Equation (2)–(5) coefficients from 294 reference stars measures (including the DR3 ICRS 2016.0 measurements), while modeling reference star parallax and proper motion. The priors for this model had the published DR3 errors. Distributions are fit with Gaussian's with standard deviations, σ, indicated in each panel.

astrometry has improved the precision of RV-derived orbital parameters, significantly reducing the 1σ errors on P_b, ϵ_b, K_b, ω_b, and T_b, listed in Table 3. For 14 Her c we find improvements in all but ϵ_c and ω_c.

The mutual inclination, Φ, of the b and c orbits can be determined through (Kopal 1959; Muterspaugh et al. 2006)

$$\cos\Phi = \cos i_b \cos i_c + \sin i_b \sin i_c \cos(\Omega_b - \Omega_c) \quad (9)$$

where i_b and i_c are the orbital inclinations, and Ω_b and Ω_c are the longitudes of their ascending nodes. Our modeling yields a significant lack of coplanarity with $\Phi = 62° \pm 12°$. Figure 6 shows the perturbation due to both companions, the epochs of observation and the residuals. We have collapsed the final 106 residuals from 17 FGS epochs, first by averaging the 17 epochs (averaging five residuals per epoch) down to 17 residuals, We then averaged the epochs 1–6, epochs 7–9, and epochs 10–17 residuals to obtain the plotted values. The (effectively) three FGS epochs provide a substandard observation set for orbit determination. The 1991.25 Hipparcos, 2015.0 DR1, and 2016.0 DR3 epochs improve the parameter accuracy and errors, providing, combined with the FGS epochs, over five wraps of the orbit for P_b.

Table 9
Reference Frame Statistics, 14 Her Parallax, and Proper Motion

Parameter	Value
Study duration	24.75 y
Number of observation sets	18
Reference star $\langle V \rangle$	12.79
Reference star $\langle (B-V) \rangle$	0.81
HST: model without 14 Her b, c orbits or 14 Her DR3 priors	
χ^2/DOF	0.617
Absolute ϖ	54.15 ± 0.22 mas
Relative μ_α	132.84 ± 0.13 mas yr^{-1}
Relative μ_δ	-297.60 ± 0.06 mas yr^{-1}
$\boldsymbol{\mu} = 325.90$ mas yr^{-1}	
P.A. $= 155.^\circ 95$	
HST: model with 14 Her b, c orbits, no 14 Her DR3 priors	
χ^2/DOF	0.463
Absolute ϖ	54.77 ± 0.22 mas
Relative μ_α	132.44 ± 0.2 mas yr^{-1}
Relative μ_δ	-298.00 ± 0.1 mas yr^{-1}
$\boldsymbol{\mu} = 326.11$ mas yr^{-1}	
P.A. $= 156.^\circ 04$	
DR3 catalog values	
Absolute ϖ	55.87 ± 0.02 mas
Absolute μ_α	131.75 ± 0.03 mas yr^{-1}
Absolute μ_δ	-297.03 ± 0.04 mas yr^{-1}
$\boldsymbol{\mu} = 324.93$ mas yr^{-1}	
P.A. $= 156.^\circ 08$	

Table 10
14 Her b, c Orbital Parameters from Astrometry and RV

Parameter	b	c
P [days]	1767.56 ± 0.22	52160 ± 1028
P [yr]	4.8393 ± 0.0006	142.8 ± 2.8
T [days]	51368.0 ± 0.5	51779 ± 33
e	0.372 ± 0.001	0.65 ± 0.06
ω [°]	22.28 ± 0.15	0 ± 1
K [m s^{-1}]	90.38 ± 0.15	50.8 ± 0.4
α [mas]	1.28 ± 0.1	10.3 ± 0.7
Ω [°]	276 ± 5	224 ± 9
i [°]	35.7 ± 3.2	82 ± 14
Derived parameters		
α [au]	0.0233 ± 0.0019	0.187 ± 0.012
a [au]	2.82	27
a [″]	0.155	1.48
$\mathcal{M} \sin i$ [$\mathcal{M}_{\rm Jup}$]	4.95	7.12
$\mathcal{M}$ [$\mathcal{M}_{\rm Jup}$]	$8.5^{+1.0}_{-0.8}$	$7.1^{+1.0}_{-0.6}$
$\mathcal{M}$ [$\mathcal{M}_\odot$]	0.0081	0.0068
Φ[a][°]	62 ± 12	

Note.
[a] Mutual inclination from Equation (9).

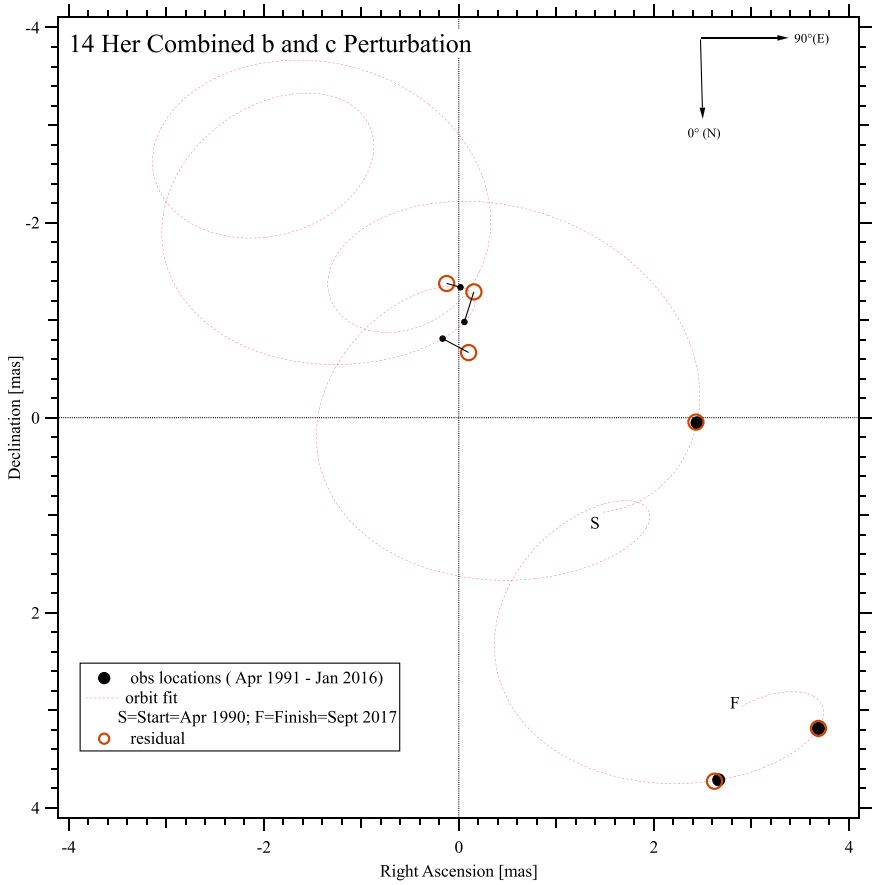

Figure 6. Residuals to the 14 Her b and c perturbation described by the Table 10 final orbital elements. Normal points (∘), as described in Section 4, are near their calculated locations (FGS •; HIPP, DR1, DR2•) on the orbit. The residual rms is 0.15 mas in R.A. and 0.13 mas in decl.

Table 11
KS Test Results

Test	D	C	α	PV
FGS versus Feng22	0.33	0.39	0.050	0.090
Feng22 versus 6th Cat.	0.20	0.11	0.050	0.000
FGS versus 6th Cat.	0.44	0.38	0.050	0.005

To determine a 14 Her b mass we find an $\mathcal{M}_b$, which satisfies this relation (Heintz 1978)

$$f(\mathcal{M}) = (\mathcal{M}_b \sin i)^3 / (\mathcal{M}_* + \mathcal{M}_b)^2 \quad (10)$$

$$R = 1.036 \times 10^{-7} K_p P (1 - \epsilon^2)^{3/2} \quad (11)$$

$$f(M) = R. \quad (12)$$

The planetary mass depends on the mass of the primary star. Assuming $\mathcal{M}_* = 0.98 \pm 0.04\ \mathcal{M}_\odot$ (Bardalez Gagliuffi et al. 2021), our orbit yields $\mathcal{M}_b = 8.5^{+1.0}_{-0.8}\ \mathcal{M}_{Jup}$. A similar analysis for 14 Her c yields $\mathcal{M}_c = 7.1^{+1.0}_{-0.6}\ \mathcal{M}_{Jup}$.

Modeling only the 14 Her b perturbation while including DR3 parallax and proper motion priors for 14 Her increases the χ^2/DOF by a factor of 3.7, yielding similar perturbation parameters, but with significantly increased parameter errors. Hence, for 14 Her b,c we adopt orbit results without DR3 priors for 14 Her.

4.2. 14 Her d

Candidate 14 Her d, with $P \sim 3765^d$, producing an RV amplitude of $K_d = 3.8$ m s^{-1}, would have an $\mathcal{M} \sin i \sim 0.28 \mathcal{M}_{Jup}$ minimum mass, which for a circular orbit would produce a perturbation, $\alpha_d = 70$ μas, undetectable with FGS data. Attempts to solve for an astrometric signature (perturbation orbit size, α, inclination, i, Ω, longitude of ascending node) for 14 Her d were unsuccessful.

Many stars produce long-period cycles of activity (e.g., Baliunas et al. 1995), and these cycles can affect RV measurements (Costes et al. 2021). Longer-period activity cycles are more likely for longer stellar rotation periods (Oláh et al. 2016). Does sufficient evidence exist to unambiguously ascribe the $P \sim 3765^d$ RV signal to a stellar activity cycle? Hirsch et al. (2021), working with an activity parameter derived from the strengths of the Calcium H and K lines, S_{HK}, find a $P \sim 3440^d$, a variation directly attributable to stellar activity. For 14 Her, $\langle S_{HK} \rangle = 0.151$ (Duncan et al. 1991). The Sun has $\langle S_{HK} \rangle = 0.170$ (Hall et al. 2009; Egeland et al. 2017). Bardalez Gagliuffi et al. (2021) list another activity parameter for 14 Her, $\log R'_{HK} = -4.94$ (Morris et al. 2019). For the Sun $\log R'_{HK} = -4.96$ (Hall et al. 2009). The rotation periods for 14 Her and the Sun are $P_{rot} = 29\overset{d}{.}5$ and $P_{rot} = 27\overset{d}{.}3$ with similar estimated ages of 4.6 Gyr (Bardalez Gagliuffi et al. 2021; Bonanno et al. 2002). The Sun has a sunspot cycle with an average period, $P \sim 11$ yr, with a range 8–17 yr (Hathaway 2015; Usoskin et al. 2021). Given the activity level agreement between the Sun and 14 Her, the 14 Her RV signal

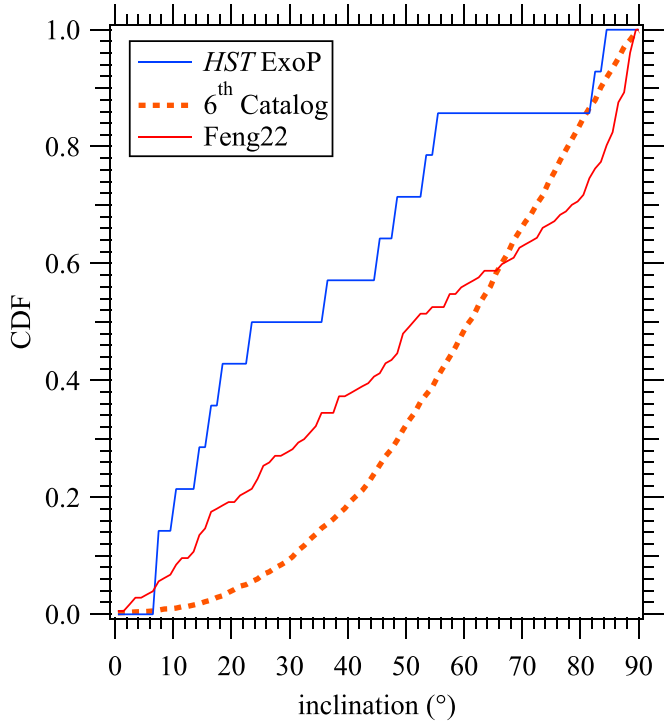

Figure 7. CDFs for: the entire inclination set from the 6th Visual Binary Star Catalog (Hartkopf et al. 2001); exoplanet perturbation inclinations (Benedict et al. 2022b; Table 11); now including 14 Her b,c; and exoplanet perturbation inclinations from Feng et al. (2022). KS test results indicate that neither our exoplanet inclination distributions nor the Feng et al. (2022) inclination distributions are drawn from the same parent population as the 6th Catalog binary inclination population, presumed to be random.

for candidate d ($P_d = 10.4$ yr) seems more likely activity than a perturbation.

We hypothesize that the activity period disagreement between Hirsch et al. (2021) and that from Section 2 might come from our access to additional HET RV data. We also included earlier, less precise ELODIE RV measurements, which extended the RV time span by over 9 yr.

5. Discussion

The Table 10 astrometry-derived parameters, α, i, and Ω values for the 14 Her b,c perturbations differ from Feng et al. (2022), but agree more closely with Bardalez Gagliuffi et al. (2021). The MCMC sampling approach used by Bardalez Gagliuffi et al. (2021) also finds a significant mutual inclination, $\Phi = 96^{+29}_{-37}°$, in general agreement with our value, $\Phi = 62° \pm 12°$. Using Equation (9) and Feng et al. (2022) values yields a smaller mutual inclination, $\Phi = 20° \pm 2°$.

Our $\mathcal{M}_b$ and $\mathcal{M}_c$ values (Table 10) agree with Bardalez Gagliuffi et al. (2021) within their respective errors, and agree for $\mathcal{M}_b$ with Feng et al. (2022). Regarding $\mathcal{M}_c$, both our and that of Bardalez Gagliuffi et al. (2021) disagree with the Feng et al. (2022) value, $\mathcal{M}_c = 5.0^{+1.1}_{-0.9}$, understandable given the Feng et al. (2022) far shorter period for 14 Her c, $P_c = 15732^{+1896}_{-2654}$ days.

Benedict et al. (2017) reviews HST FGS past astrometry to characterize the perturbations due to candidate planets. More recent results include masses for HD202206 B and c, a circumbinary brown-dwarf system (Benedict & Harrison 2017), and null results for companions to μ Ara of any mass (Benedict et al. 2022b). During the publication process for the latter paper, a referee pointed out the possibility that inclinations obtained with FGS astrometry were biased toward low values. We explored this at length in Benedict et al. (2022b), but could not identify any flaws in our modeling. Our agreement with Bardalez Gagliuffi et al. (2021) for 14 Her b,c provides additional support for the soundness of our analyses.

However, to further explore this possible bias, we compare, via a Kolmogorov–Smirnov (K-S) test, a cumulative distribution function (CDF) for 177 companion inclinations in Feng et al. (2022) to our FGS-derived inclinations, now including the 14 Her b,c results. To produce the CDF we put all inclinations on a 0°–90° scale by applying an offset to inclinations over 90°; $i_{corr} = 90° - \mathrm{mod}(i, 90°)$. A K-S test produces a test statistic, D, a critical value, C, and a p value, PV. Values of D less than C support the null hypothesis, as does a p value larger than an adopted significance level, $\alpha = 0.05$. The K-S test of FGS against Feng et al. (2022) inclinations suggest that both samples were drawn from the same parent distribution, D less than C with PV $> \alpha$ (Table 11).

We then compare the Feng et al. (2022) inclinations with a set of 3214 binary star inclinations, presumed to be purely random in distribution (6th Catalog of Visual Binary Stars; Hartkopf et al. 2001). We find the null hypothesis that Feng et al. (2022) inclinations are as random as the 6th Catalog inclinations is not supported, D marginally larger than C, and the PV far lower than the significance level, α (Table 11). Similarly retesting the FGS-derived inclinations continues to indicate a bias to lower inclinations. Both the FGS and the Feng et al. (2022) inclinations seem inconsistent with a sample with a random distribution of inclinations. We show these CDF in Figure 7. These K-S tests suggest either that observed exoplanetary systems, first discovered via RV, have astrometrically measured inclinations with a real bias toward smaller values, or that both Feng et al. (2022) and the FGS have unresolved issues with their analyses. See Pourbaix (2001) for one possible explanation and Benedict et al. (2022a; Section 5.2.2) for a counter argument in support of the FGS.

6. Summary

For the 14 Her system from modeling 25 yr of ground-based RV and the results from models which utilizes 17 epochs of HST/FGS, one epoch each of Gaia DR1 and DR3, and one epoch of Hipparcos astrometry all spanning 25.75 yr, we find:

1. Derived from only the augmented body of RV data now including HET measurements, improved companion orbital elements (P, ϵ, ω, T_0, K);
2. After subtracting the 14 Her b and c RV signals, evidence for a signal with $P \sim 3765^d$, tentatively identified as an activity cycle;
3. From a model containing no proper motion, no parallax priors, nor perturbing 14 Her b,c orbits for 14 Her a parallax, $\pi_{abs} = 54.14 \pm 0.22$ mas, disagreeing with the Gaia DR3 value, and a proper motion relative to a Gaia DR3 reference frame, $\boldsymbol{\mu} = 325.90$ mas yr^{-1} with a position angle, P.A. $= 155°.95$, differing by $+0.97$ mas yr^{-1} and $-0°.13$ compared to Gaia DR3;
4. From a model containing neither 14 Her proper motion nor parallax priors but with perturbing 14 Her b, c orbits for 14 Her, a parallax, $\pi_{abs} = 54.77 \pm 0.22$ mas, and a proper motion relative to a Gaia DR3 reference frame, $\boldsymbol{\mu} = 326.11$ mas yr^{-1} with a position angle, P.

A. $= 156.^{\circ}04$, differing by -1.2 mas yr^{-1} and $+0.^{\circ}04$ compared to Gaia DR3;

5. That model, using the RV-derived $P_{b,c}$, $\epsilon_{b,c}$, $K_{b,c}$, $\omega_{b,c}$, and $T_{b,c}$ orbital parameters as observations with error, yields $\alpha_b = 1.3 \pm 0.1$ mas, $i_b = 35.^{\circ}7 \pm 3.^{\circ}2$, $\Omega_b = 276^{\circ} \pm 5^{\circ}$, and $\alpha_c = 10.3 \pm 0.7$ mas, $i_c = 82^{\circ} \pm 14^{\circ}$, $\Omega_c = 224^{\circ} \pm 9^{\circ}$ with errors on P, ϵ, K, ω, and T smaller than those obtained only from RV;
6. A mass for 14 Her b, $\mathcal{M}_b = 8.5^{+1.0}_{-0.8}$ $\mathcal{M}_{Jup}$, and for 14 Her c, $\mathcal{M}_c = 7.1^{+1.0}_{-0.6}$ $\mathcal{M}_{Jup}$;
7. A significant lack of coplanarity with $\Phi = 62^{\circ} \pm 12^{\circ}$.

A combination of FGS and RV data with future Gaia data releases can produce significantly improved companion orbits and masses for 14 Her b and c, and confirm a stellar activity source for the $P \sim 3780$ days RV signal.

All exoplanetary systems investigated through HSTFGS astrometry were first identified as possible targets via RV, as were the systems investigated in Feng et al. (2022). We find evidence that these two independent investigations of exoplanet host stars have companions that exhibit a bias toward lower inclinations. Perhaps a large number of systems discovered by Gaia, without previous RV evidence for their existence, can assist in identifying a cause for this bias.

We thank the anonymous referee for their suggestions. This work is based on observations made with the NASA/ESA Hubble Space Telescope, obtained at the Space Telescope Science Institute. Support for this work was provided by NASA through grants 11210 and 11788 from the Space Telescope Science Institute, which is operated by the Association of Universities for Research in Astronomy, Inc., under NASA contract NAS5-26555. This research has made use of the *SIMBAD* and *Vizier* databases, operated at Centre Donnees Stellaires, Strasbourg, France; Aladin, developed and maintained at CDS; and NASA's truly essential Astrophysics Data System Abstract Service. This work has made use of data from the European Space Agency (ESA) mission Gaia (http://www.cosmos.esa.int/gaia), processed by the Gaia Data Processing and Analysis Consortium (DPAC; http://www.cosmos.esa.int/web/gaia/dpac/consortium). Funding for the DPAC has been provided by national institutions, in particular the institutions participating in the Gaia Multilateral Agreement. G.F.B. thanks Dr. Paul Butler for cheerfully offered observation accounting assistance. Thanks to Dr. Tom Harrison for securing the reference star $B - V$ photometry.

ORCID iDs

G. F. Benedict https://orcid.org/0000-0003-2852-3279
E. P. Nelan https://orcid.org/0000-0002-5704-5221
J. L. Bean https://orcid.org/0000-0003-4733-6532

References

Baliunas, S. L., Donahue, R. A., Soon, W. H., et al. 1995, ApJ, 438, 269
Bardalez Gagliuffi, D. C., Faherty, J. K., Li, Y., et al. 2021, ApJL, 922, L43
Bean, J. L., McArthur, B. E., Benedict, G. F., et al. 2007, AJ, 134, 749
Benedict, G. 2005, Astrometric Masses of Extrasolar Planets and Brown Dwarfs HST Proposal ID 10610, Univ. Texas at Austin https://archive.stsci.edu/proposal_search.php?id=10610&mission=hst
Benedict, G. F., Barnes, T. G., Evans, N. R., et al. 2022a, AJ, 163, 282
Benedict, G. F., & Harrison, T. E. 2017, AJ, 153, 258
Benedict, G. F., Henry, T. J., Franz, O. G., et al. 2016, AJ, 152, 141
Benedict, G. F., McArthur, B. E., Bean, J. L., et al. 2010, AJ, 139, 1844
Benedict, G. F., McArthur, B. E., Feast, M. W., et al. 2007, AJ, 133, 1810
Benedict, G. F., McArthur, B. E., Feast, M. W., et al. 2011, AJ, 142, 187
Benedict, G. F., McArthur, B. E., Franz, O. G., et al. 2001, AJ, 121, 1607
Benedict, G. F., McArthur, B. E., Gatewood, G., et al. 2006, AJ, 132, 2206
Benedict, G. F., McArthur, B. E., Nelan, E. P., et al. 2017, PASP, 129, 012001
Benedict, G. F., McArthur, B. E., Nelan, E. P., et al. 2022b, AJ, 163, 295
Bonanno, A., Schlattl, H., & Paternò, L. 2002, A&A, 390, 1115
Brandt, T. D. 2021, ApJS, 254, 42
Butler, R. P., Marcy, G. W., Vogt, S. S., et al. 2003, ApJ, 582, 455
Costes, J. C., Watson, C. A., de Mooij, E., et al. 2021, MNRAS, 505, 830
Duncan, D. K., Vaughan, A. H., Wilson, O. C., et al. 1991, ApJS, 76, 383
Egeland, R., Soon, W., Baliunas, S., et al. 2017, ApJ, 835, 25
Feng, F., Butler, R. P., Vogt, S. S., et al. 2022, ApJS, 262, 21
Ford, E. B. 2006, in, in ASP Conf. Ser. 352, What Do Multiple Planet Systems Teach Us about Planet Formation?, ed. K. Sheila, R. Seth, K.-S. Jacqueline, L. Martin, & D. Niv (San Francisco, CA: ASP), 15
Gaia Collaboration, Vallenari, A., Brown, A. G. A., et al. 2022, arXiv:2208.00211
Goździewski, K., Konacki, M., & Maciejewski, A. J. 2006, ApJ, 645, 688
Hall, J. C., Henry, G. W., Lockwood, G. W., et al. 2009, AJ, 138, 312
Hartkopf, W. I., Mason, B. D., & Worley, C. E. 2001, AJ, 122, 3472
Hathaway, D. H. 2015, LRSP, 12, 4
Heintz, W. D. 1978, Double Stars (Dordrecht: Reidel)
Henry, G. W., Kane, S. R., Wang, S. X., et al. 2013, ApJ, 768, 155
Hirsch, L. A., Rosenthal, L., Fulton, B. J., et al. 2021, AJ, 161, 134
Holtzman, J. A., Harrison, T. E., & Coughlin, J. L. 2010, AdAst, 2010, 193086
Jefferys, W. H., Fitzpatrick, M. J., & McArthur, B. E. 1988, CeMec, 41, 39
Kopal, Z. 1959, Close Binary Systems (London: Chapman and Hall)
Lindegren, L., Lammers, U., Bastian, U., et al. 2016, A&A, 595, A4
Martioli, E., McArthur, B. E., Benedict, G. F., et al. 2010, ApJ, 708, 625
McArthur, B. E., Benedict, G. F., Barnes, R., et al. 2010, ApJ, 715, 1203
McArthur, B. E., Benedict, G. F., Henry, G. W., et al. 2014, ApJ, 795, 41
McArthur, B. E., Benedict, G. F., Jefferys, W. J., et al. 2006, in The 2005 HST Calibration Workshop: Hubble After the Transition to Two-Gyro Mode, ed. A. M. Koekemoer, P. Goudfrooij, & L. L. Dressel (Washington, DC: NASA), 396
Morris, B. M., Curtis, J. L., Sakari, C., et al. 2019, AJ, 158, 101
Muterspaugh, M. W., Lane, B. F., Konacki, M., et al. 2006, ApJ, 636, 1020
Naef, D., Mayor, M., Beuzit, J. L., et al. 2004, A&A, 414, 351
Nelan, E. 2015, Fine Guidance Sensor Instrument Handbook v.23.0
Oláh, K., Kővári, Z., Petrovay, K., et al. 2016, A&A, 590, A133
Pourbaix, D. 2001, A&A, 369, L22
Pourbaix, D., & Jorissen, A. 2000, A&AS, 145, 161
Rosenthal, L. J., Fulton, B. J., Hirsch, L. A., et al. 2021, ApJS, 255, 8
Standish, E. M., Jr. 1990, A&A, 233, 252
Stassun, K. G., & Torres, G. 2021, ApJL, 907, L33
Tull, R. G. 1998, Proc. SPIE, 3355, 387
Usoskin, I. G., Solanki, S. K., Krivova, N. A., et al. 2021, A&A, 649, A141
van de Kamp, P. 1967, Principles of Astrometry (San Francisco, CA: Freeman)
van Leeuwen, F. 2007, Hipparcos, the New Reduction of the Raw Data (Berlin: Springer)
Vogt, S. S., Radovan, M., Kibrick, R., et al. 2014, PASP, 126, 359
Wittenmyer, R. A., Endl, M., & Cochran, W. D. 2007, ApJ, 654, 625
Wright, J. T., Marcy, G. W., Fischer, D. A., et al. 2007, ApJ, 657, 533
Wright, J. T., Upadhyay, S., Marcy, G. W., et al. 2009, ApJ, 693, 1084